



This is a repository copy of *Controllability analysis and controller design for variable-pitch propeller quadcopters with one propeller failure*.

White Rose Research Online URL for this paper:  
<https://eprints.whiterose.ac.uk/157799/>

Version: Accepted Version

---

**Article:**

Wang, Z., Groß, R. [orcid.org/0000-0003-1826-1375](https://orcid.org/0000-0003-1826-1375) and Zhao, S. (2020) Controllability analysis and controller design for variable-pitch propeller quadcopters with one propeller failure. *Advanced Control for Applications: Engineering and Industrial Systems*, 2 (2). e29. ISSN 2578-0727

<https://doi.org/10.1002/adc2.29>

---

This is the peer reviewed version of the following article: Wang, Z, Groß, R, Zhao, S. Controllability analysis and controller design for variable-pitch propeller quadcopters with one propeller failure. *Adv Control Appl*. 2020; 2:e29, which has been published in final form at <https://doi.org/10.1002/adc2.29>. This article may be used for non-commercial purposes in accordance with Wiley Terms and Conditions for Use of Self-Archived Versions. This article may not be enhanced, enriched or otherwise transformed into a derivative work, without express permission from Wiley or by statutory rights under applicable legislation. Copyright notices must not be removed, obscured or modified. The article must be linked to Wiley's version of record on Wiley Online Library and any embedding, framing or otherwise making available the article or pages thereof by third parties from platforms, services and websites other than Wiley Online Library must be prohibited.

**Reuse**

Items deposited in White Rose Research Online are protected by copyright, with all rights reserved unless indicated otherwise. They may be downloaded and/or printed for private study, or other acts as permitted by national copyright laws. The publisher or other rights holders may allow further reproduction and re-use of the full text version. This is indicated by the licence information on the White Rose Research Online record for the item.

**Takedown**

If you consider content in White Rose Research Online to be in breach of UK law, please notify us by emailing [eprints@whiterose.ac.uk](mailto:eprints@whiterose.ac.uk) including the URL of the record and the reason for the withdrawal request.



[eprints@whiterose.ac.uk](mailto:eprints@whiterose.ac.uk)  
<https://eprints.whiterose.ac.uk/>

## ARTICLE TYPE

# Controllability Analysis and Controller Design for VPP Quadcopters with one Propeller Failure

Zhikun Wang<sup>1</sup> | Roderich Groß<sup>1</sup> | Shiyu Zhao\*<sup>2</sup>

<sup>1</sup>Department of Automatic Control and Systems Engineering, The University of Sheffield, Sheffield, UK

<sup>2</sup>School of Engineering at Westlake University, Institute of Advanced Technology at Westlake Institute for Advanced Study, China

**Correspondence**

\*Shiyu Zhao, School of Engineering, Westlake University, Email: zhaoshiyu@westlake.edu.cn

**Abstract**

This paper studies a relatively new type of aerial platform: variable-pitch propeller (VPP) quadcopters. Unlike conventional fixed-pitch propellers that can only generate upward thrust forces, a VPP can adjust its pitch angle to generate either upward or downward thrust forces. This provides VPP quadcopter with high agility and strong maneuverability. Although VPP quadcopters have attracted some attention recently, their potential has not been fully explored yet. In this paper, we study the fault-tolerant property of VPP quadcopters when one of the four VPPs fails to provide any forces or torques. We identify the equilibrium state in this case and conduct the controllability analysis based on a linearised model. This shows that the system remains controllable even if one propeller fails. As a result, simple LQR controllers can be used to control the platform. Although the controllability analysis and controller are based on the linearised model, numerical simulation incorporating measurement noises and external disturbances verifies the theoretic findings.

**KEYWORDS:**

Quadcopters, Fault-Tolerant Control (FTC), Variable Pitch Propeller (VPP), Controllability Analysis

## 1 | INTRODUCTION

Quadcopter unmanned aerial vehicles (UAVs) have become a popular platform for many aerial applications such as aerial photography, surveillance, and transportation. Compared to other applications, safety-critical tasks like parcel delivery and passenger transportation pose higher requirements about the safety and reliability of the platform. To improve the safety and reliability of the quadcopter platform, there are many methods<sup>1</sup>. One of them is to apply the fault-tolerant control method, which allows the quadcopter to maintain a relatively stable state in the presence of one or more faults such as motor failures<sup>2,3</sup>. This method has attracted extensive studies due to its great importance<sup>4,5,6,7</sup>.

In this paper, we study a specific yet important type of aerial platforms: variable-pitch propeller (VPP) quadcopters. This type of platform is similar to conventional quadcopter platforms in terms both mechanical and control structures. The key difference is that a VPP can adjust its pitch angle and hence generate both upward and downward thrusts. Although the mechanics of VPPs are more complicated than conventional propellers, the overall mechanical structure and the control system structure of VPP quadcopters are the same as the conventional ones.

A slight mechanical complexity increase of the VPPs brings many interesting and attractive features. First, regarding the direction of propeller thrust forces, each VPP can generate both upward and downward thrust forces, whereas a fixed-pitch propeller of a conventional quadcopter can only generate upward thrust forces. This provides VPP quadcopters with strong maneuverability. For example, a VPP quadcopter can hover upside down, which is not feasible for conventional quadcopters.

Second, regarding the control bandwidth, the magnitude of the thrust force generated by a VPP can be adjusted efficiently by controlling the propeller pitch angle through the associated actuator of the VPP. As a comparison, a conventional quadcopter can only adjust the force magnitude of a propeller by speed control. The response of speed control is much slower than actuator control<sup>8,9</sup>. This brings high agility to VPP quadcopters. Due to these features, VPP quadcopters have attracted some attention recently<sup>10,11,12</sup>. However, their potential has not been fully explored yet.

In this paper, we explore a new fault-tolerant feature of VPP quadcopters. For conventional quadcopters, when one or more motors/propellers fail to work properly, the platforms usually become extremely hard to control and sophisticated controllers must be designed<sup>13,14</sup>. More importantly, even under fault-tolerant controllers, conventional quadcopters with faults are only able to fly in very special manners such as continuously rotating<sup>15,16,17</sup>. In contrast, VPP quadcopters shows strong fault-tolerant ability as we show in this paper.

The contributions of this paper are as follows. First, we conduct the controllability analysis of a VPP quadcopter with one propeller failure based on the linearised dynamical model. It is shown that, when one propeller fails, all states of the quadcopter remain controllable. For comparison purposes, we also analyze the controllability of fixed-pitch quadcopters with one motor failure and show that fixed-pitch quadcopters are uncontrollable with motor failures. Second, we identify the equilibrium point and derive the linearised dynamical model of VPP quadcopters. Based on the linearised model, we design an Linear–quadratic regulator (LQR) controller to handle propeller failure. Using this simple controller, the VPP quadcopter can accurately track a given trajectory even if subjected to wind disturbances or noise. This property is important for safety-critical tasks such as flying taxi, where it is necessary to transport the human passengers to a safe place securely in the presence of propeller failures. Thanks for this property, VPP quadcopters provide an important alternative platform for safety-critical aerial tasks.

It is worth mentioning that we do not consider fault detection, isolation, or switching controllers in this paper. These important topics will be addressed in our future work. The focus of this paper is to explore the fault-tolerant ability of VPP quadcopters which has not been reported in the literature.

This paper is organized as follows. Section 2 presents the dynamical model of VPP quadcopters in the presence of one propeller failure. Section 3 presents the linearised model and analyzes the system controllability. Section 4 shows comprehensive simulation results. Conclusions are drawn in Section 5.

## 2 | DYNAMIC MODEL OF VPP QUADCOPTERS

The mechanical structure of a VPP quadcopter is shown in Fig. 1. It is notable that its overall structure is the same as a conventional fixed-pitch quadcopter. The state vector is  $\mathbf{x} = [x, y, z, \phi, \theta, \psi, p, q, r, u, v, w]^T \in \mathbb{R}^{12}$ , where  $(x, y, z)$ ,  $(\phi, \theta, \psi)$ ,  $(p, q, r)$ , and  $(u, v, w)$  denote the position, attitude, angular velocity, and linear velocity, respectively. The rotation from the body frame to the global frame is described by the rotational matrix  $\mathbf{R} \in SE(3)$ . Let  $f_1, f_2, f_3, f_4$  be the forces generated by propellers 1 to 4, where propellers 1 and 3 spin clockwise and propellers 2 and 4 spin counterclockwise, and  $\tau_1, \tau_2, \tau_3, \tau_4$  be the torques generated by propellers 1 to 4, respectively.

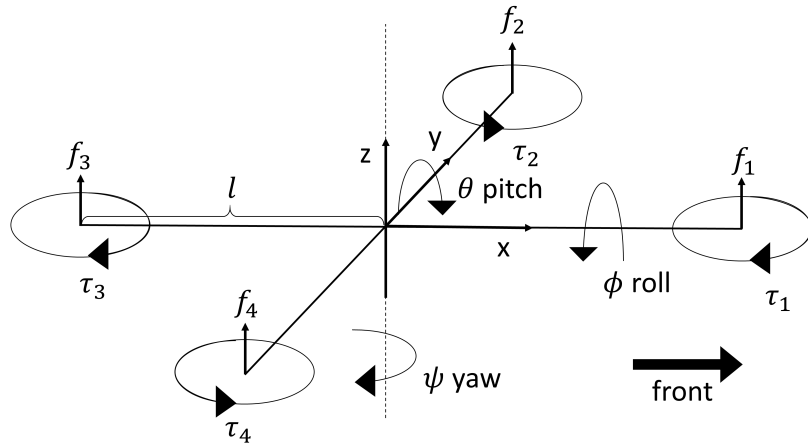


FIGURE 1 The mechanical structure of a VPP quadcopter.

The dynamics of the VPP quadcopter are described by

$$\dot{\mathbf{x}} = \begin{bmatrix} \dot{x} \\ \dot{y} \\ \dot{z} \\ \dot{\phi} \\ \dot{\theta} \\ \dot{\psi} \\ \dot{p} \\ \dot{q} \\ \dot{r} \\ \dot{u} \\ \dot{v} \\ \dot{w} \end{bmatrix} = \begin{bmatrix} u \\ v \\ w \\ p + q \sin \phi \tan \theta + r \cos \phi \tan \theta \\ q \cos \phi - r \sin \phi \\ q \sin \phi \sec \theta + r \cos \phi \sec \theta \\ qr \frac{I_z - I_y}{I_x} + u_2 \frac{l}{I_x} \\ rp \frac{I_x - I_z}{I_y} + u_3 \frac{l}{I_y} \\ pq \frac{I_y - I_x}{I_z} + u_4 \frac{l}{I_z} \\ \frac{(\cos \psi \sin \theta \cos \phi + \sin \psi \sin \phi)u_1 - d_x u}{m} \\ \frac{(\sin \psi \sin \theta \cos \phi - \cos \psi \sin \phi)u_1 - d_y v}{m} \\ (\cos \theta \cos \phi)u_1/m - d_z w/m - g \end{bmatrix}, \quad (1)$$

where  $l$  is the length of each quadcopter arm,  $m$  is the mass of the quadcopter,  $g$  denotes the gravitational constant, and  $I_x, I_y, I_z$  are the moment of inertia. In our work, suppose  $m = 1$  Kg,  $g = 10$  m<sup>2</sup>/s, and  $l = 0.35$  m.

The control inputs,  $\mathbf{u} = [u_1, u_2, u_3, u_4]^T \in \mathbb{R}^4$ , are

$$\mathbf{u} = \begin{bmatrix} u_1 \\ u_2 \\ u_3 \\ u_4 \end{bmatrix} = \begin{bmatrix} f_1 + f_2 + f_3 + f_4 \\ f_3 - f_1 \\ f_4 - f_2 \\ \tau_1 - \tau_2 + \tau_3 - \tau_4 \end{bmatrix}. \quad (2)$$

The pitch angle of VPP propeller  $i$  is denoted as  $\alpha_i$ , which could be positive or negative. The spinning speed of motor  $i$  is  $\omega_i$ , which is positive. The force and torque generated by VPP propeller  $i$  are

$$\begin{aligned} f_i &= k_1 \omega_i^2 \alpha_i, \\ \tau_i &= k_2 \omega_i^2 + k_3 \omega_i^2 \alpha_i^2 + k_4 \omega_i \alpha_i, \end{aligned} \quad (3)$$

where  $k_1, k_2, k_3, k_4$  are constant parameters determined by the motor and air resistance<sup>18,19</sup>. In our work, suppose  $k_1 = 5 \times 10^{-7}$ ,  $k_2 = 1 \times 10^{-8}$ ,  $k_3 = 2 \times 10^{-10}$ , and  $k_4 = 4 \times 10^{-7}$ . Note that the torque generated by a VPP can be nonzero even when the pitch angle and its force are zero.

There are two types of power supply modes for VPP quadcopters. One is the centralized power mode, where the spin of all propellers is powered by a central motor placed at the centre of the quadcopter. In this case, all the propellers have the same and fixed spinning speed<sup>20</sup>. The other is the decentralized power mode, where the spin of each propeller is powered by an independent motor. In this case, the spinning speeds of different propellers may be different<sup>9</sup>. In this paper, we consider the decentralized power mode, where both  $\alpha_i$  and  $\omega_i$  can be adjusted independently by each propeller. In this work, suppose that the maximum spinning speed of each independent motor is 10,000 RPM, and the pitch angle of each propeller varies in the interval of  $[-15, 15]$  deg ( $[-0.26, 0.26]$  rad). Substituting (3) into (2) gives

$$\begin{aligned} u_1 &= k_1(\omega_1^2 \alpha_1 + \omega_2^2 \alpha_2 + \omega_3^2 \alpha_3 + \omega_4^2 \alpha_4), \\ u_2 &= k_1(\omega_3^2 \alpha_3 - \omega_1^2 \alpha_1), \\ u_3 &= k_1(\omega_4^2 \alpha_4 - \omega_2^2 \alpha_2), \\ u_4 &= k_2(\omega_3^2 + \omega_1^2 - \omega_2^2 - \omega_4^2) + \\ &\quad k_3(\omega_3^2 \alpha_3^2 + \omega_1^2 \alpha_1^2 - \omega_2^2 \alpha_2^2 - \omega_4^2 \alpha_4^2) + \\ &\quad k_4(\omega_3 \alpha_3 + \omega_1 \alpha_1 - \omega_2 \alpha_2 - \omega_4 \alpha_4). \end{aligned}$$

When there is a propeller failure,  $\mathbf{u}$  would be different. Without loss of generality, suppose propeller 1 fails such that it provides zero force and zero torque. That is  $f_1$  and  $\tau_1$  are always zero. Then,  $\mathbf{u}$  becomes

$$\begin{aligned} u_1 &= k_1(\omega_2^2\alpha_2 + \omega_3^2\alpha_3 + \omega_4^2\alpha_4), \\ u_2 &= k_1\omega_3^2\alpha_3, \\ u_3 &= k_1(\omega_4^2\alpha_4 - \omega_2^2\alpha_2), \\ u_4 &= k_2(\omega_3^2 - \omega_2^2 - \omega_4^2) + \\ &\quad k_3(\omega_3^2\alpha_3^2 - \omega_2^2\alpha_2^2 - \omega_4^2\alpha_4^2) + \\ &\quad k_4(\omega_3\alpha_3 - \omega_2\alpha_2 - \omega_4\alpha_4). \end{aligned} \quad (4)$$

Although propeller 1 fails, there remain six independent control quantities,  $\omega_2, \omega_3, \omega_4$  and  $\alpha_2, \alpha_3, \alpha_4$ . To generate desired  $\mathbf{u}$ , the six control quantities are still redundant, which is the fundamental reason why the system remain controllable in the presence of a propeller failure.

### 3 | LINEARISATION AND CONTROLLABILITY ANALYSIS

In this section, we identify the equilibrium point of the system in the presence of a propeller failure, linearise the system at the equilibrium point, and conduct controllability analysis. To limit the risk of excessive vibration or propeller stall<sup>8</sup>, we assume that all  $\omega_i$  are bounded by  $[0, 10000]$  rpm and all  $\alpha_i$  are bounded by  $[-0.26, 0.26]$  rad.

#### 3.1 | Equilibrium Point

Consider a desired state

$$\mathbf{x}^* = [x^*, y^*, z^*, 0, 0, \psi^*, 0, 0, 0, 0, 0]^T.$$

In order to keep the system at this state, the input must be

$$\mathbf{u}^* = [mg, 0, 0, 0]^T. \quad (5)$$

Substituting (5) into (4) yields

$$mg = k_1\omega_2^2\alpha_2 + k_1\omega_3^2\alpha_3 + k_1\omega_4^2\alpha_4, \quad (6)$$

$$0 = k_1\omega_3^2\alpha_3, \quad (7)$$

$$0 = k_1\omega_4^2\alpha_4 - k_1\omega_2^2\alpha_2, \quad (8)$$

$$\begin{aligned} 0 &= k_2(\omega_3^2 - \omega_2^2 - \omega_4^2) + \\ &\quad k_3(\omega_3^2\alpha_3^2 - \omega_2^2\alpha_2^2 - \omega_4^2\alpha_4^2) + \\ &\quad k_4(\omega_3\alpha_3 - \omega_2\alpha_2 - \omega_4\alpha_4). \end{aligned} \quad (9)$$

The next step is to solve the above equations. Equation (7) implies that  $\omega_3^2\alpha_3 = 0$ . It is implied from (9) that  $\omega_3 \neq 0$ ; otherwise, the right-hand side of (9) is less than zero. As a result, we know  $\alpha_3 = 0$  and  $\omega_3 \neq 0$ , which means propeller 3 still spins but with zero pitch angle. On the other hand, equations (6), (7) and (8) imply

$$k_1\omega_2^2\alpha_2 = k_1\omega_4^2\alpha_4 = \frac{mg}{2}, \quad (10)$$

which means propellers 2 and 4 provide forces to counter gravity. Without loss of generality, suppose

$$\omega_2 = \omega_4. \quad (11)$$

As a result,

$$\alpha_2 = \alpha_4, \quad (12)$$

Substituting (11) and (12) into (9) gives

$$k_2\omega_3^2 = 2(k_2\omega_2^2 + k_3\omega_2^2\alpha_2^2 + k_4\omega_2\alpha_2). \quad (13)$$

Substituting (10) to (13) yields

$$k_2\omega_3^2 = 2 \left[ k_2\omega_2^2 + \frac{k_3}{k_1^2} \left( \frac{mg}{2\omega_2} \right)^2 + \frac{k_4mg}{2k_1\omega_2} \right] := r(\omega_2), \quad (14)$$

where  $r(\omega_2)$  represents the right-hand side of (14).

Next we identify the range of the value of  $r(\omega_2)$ . The derivative of  $r(\omega_2)$  with respect to  $\omega_2$  is

$$\frac{dr(\omega_2)}{d\omega_2} = 2 \left( 2k_2\omega_2 - \frac{k_3m^2g^2}{2k_1^2\omega_2^3} - \frac{k_4mg}{2k_1\omega_2^2} \right). \quad (15)$$

By analyzing (15), we notice that  $r(\omega_2)$  is a monotonically increasing function when  $\omega_2 \in [0, 10000]$ . In addition, equation (10) implies that, when the pitch angle takes the maximum value  $\alpha_2 = 0.26$ , the rotating speed would take the minimum value  $\omega_2 = 6201$ . As a result,  $\omega_2 \in [6201, 10000]$ . Substituting the interval into (14) gives  $r(\omega_2) \in [0.7714, 2]$ . Meanwhile, the left-hand side of (14) satisfies  $k_2\omega_3^2 \in [0, 1]$  when  $\omega_3 \in [0, 10000]$ . By combining the bounds of the left- and right-hand sides of (14), we know

$$k_2\omega_3^2 = r(\omega_2) \in [0.7714, 1]. \quad (16)$$

Substituting (16) to (14) yields  $\omega_2 \in [6201, 7067]$  and  $\omega_3 \in [8782, 10000]$ . We simply choose  $\omega_3 = 9000$ , a intermediate value in  $[8782, 10000]$ . Note that  $\omega_3$  remains constant all the time.

By substituting  $\omega_3 = 9000$  into (14), we can obtain four solutions:  $\omega_2^* = -217, 227, 6355$ , and  $-6365$ . As  $\omega_2 \in [6201, 7067]$  as aforementioned,  $\omega_2^* = 6355$  is the only feasible solution. Then, substituting  $\omega_2^*$  into (10) gives  $\alpha_2^* = 0.2476$ .

Let  $\mathbf{z} = [\omega_2, \alpha_2, \alpha_3, \alpha_4]^T$ . It follows from the above analysis that, in order to keep the system at the state  $\mathbf{x}^*$ ,  $\mathbf{z}$  should be

$$\begin{aligned} \mathbf{z}^* &= [\omega_2^*, \alpha_2^*, \alpha_3^*, \alpha_4^*]^T \\ &= [6355, 0.2476, 0, 0.2476]^T. \end{aligned}$$

### 3.2 | Linearised Model

To linearise the nonlinear dynamical system, consider  $\bar{\mathbf{z}} = \mathbf{z} - \mathbf{z}^*$  and  $\bar{\mathbf{x}} = \mathbf{x} - \mathbf{x}^*$ . Let  $\mathbf{F}(\bar{\mathbf{x}}, \bar{\mathbf{z}}) \in \mathbb{R}^{12}$  be the right-hand side of (1). Then, the linearised model is

$$\dot{\bar{\mathbf{x}}} = \mathbf{A}\bar{\mathbf{x}} + \mathbf{B}\bar{\mathbf{z}},$$

where

$$\begin{aligned} \mathbf{A} &= \left. \frac{\partial \mathbf{F}(\bar{\mathbf{x}}, \bar{\mathbf{z}})}{\partial \mathbf{x}} \right|_{\mathbf{x}=\mathbf{x}^*, \mathbf{z}=\mathbf{z}^*} \\ &= \begin{bmatrix} \mathbf{0}_{3 \times 3} & \mathbf{0}_{3 \times 3} & \mathbf{0}_{3 \times 3} & \mathbf{I}_{3 \times 3} \\ \mathbf{0}_{3 \times 3} & \mathbf{0}_{3 \times 3} & \mathbf{I}_{3 \times 3} & \mathbf{0}_{3 \times 3} \\ \mathbf{0}_{3 \times 3} & \mathbf{0}_{3 \times 3} & \mathbf{0}_{3 \times 3} & \mathbf{0}_{3 \times 3} \\ \mathbf{0}_{3 \times 3} & \mathbf{E}_{3 \times 3} & \mathbf{0}_{3 \times 3} & \mathbf{0}_{3 \times 3} \end{bmatrix} \in \mathbb{R}^{12 \times 12}, \\ \mathbf{E}_{3 \times 3} &= \begin{bmatrix} g \sin \psi^* & g \cos \psi^* & 0 \\ -g \cos \psi^* & g \sin \psi^* & 0 \\ 0 & 0 & 0 \end{bmatrix}, \end{aligned}$$

and

$$\mathbf{B} = \left. \frac{\partial \mathbf{F}(\bar{\mathbf{x}}, \bar{\mathbf{z}})}{\partial \mathbf{z}} \right|_{\mathbf{x}=\mathbf{x}^*, \mathbf{z}=\mathbf{z}^*} = \begin{bmatrix} 0 & 0 & 0 & 0 \\ 0 & 0 & 0 & 0 \\ 0 & 0 & 0 & 0 \\ 0 & 0 & 0 & 0 \\ 0 & 0 & 0 & 0 \\ 0 & 0 & 0 & 0 \\ 0 & h_3 \frac{l}{I_x} & 0 & 0 \\ -h_2 \frac{l}{I_y} & 0 & -h_4 \frac{l}{I_y} & n_4 - n_2 \\ -m_2 & m_3 & -m_4 & -o_2 - o_4 \\ 0 & 0 & 0 & 0 \\ 0 & 0 & 0 & 0 \\ \frac{k_1}{m} \omega_2^{*2} & \frac{k_1}{m} \omega_3^{*2} & \frac{k_1}{m} \omega_4^{*2} & p_4 + p_2 \end{bmatrix} \in \mathbb{R}^{12 \times 4},$$

with

$$\begin{aligned} h_i &= k_1 \omega_i^{*2}, \\ m_i &= 2k_3 \alpha_i^* \omega_i^{*2} + k_4 \omega_i^*, \\ n_i &= 2k_1 \alpha_i^* \omega_i^* \frac{l}{I_y}, \\ o_i &= (2k_2 \omega_i^* + 2k_3 \omega_i^* \alpha_i^{*2} + k_4 \alpha_i^*) \frac{l}{I_z}, \\ p_i &= 2 \frac{k_1}{m} \omega_i^* \alpha_i^*. \end{aligned}$$

### 3.3 | Controllability Analysis of VPP Quadcopters

It can be calculated that the rank of the controllability matrix is  $\text{rank}(\mathbf{Q}) = \text{rank}[\mathbf{B} \ \mathbf{A}\mathbf{B} \ \mathbf{A}^2\mathbf{B} \ \dots \ \mathbf{A}^{11}\mathbf{B}] = 12$ . As a result, the controllability matrix is of full row rank. Hence, all the states remain controllable when one propeller fails. Although the controllability is analysed based on the linearised system, we show later by simulation that the nonlinear model of a VPP quadcopter can be fully controlled around the equilibrium point. This is a significant advantage of VPP quadcopters compared to the conventional ones. The fundamental reason of this advantage is that the VPP control system has eight independent control inputs whereas a conventional quadcopter only has four. In the future, we will study control of VPP quadcopters subject to two or more propeller failures.

### 3.4 | Controllability Analysis of Conventional Quadcopters

For comparison purposes, we analyse the controllability of conventional fixed-pitch quadcopters with one motor failure in this section. We consider a specific mechanical configuration where motors located on arms with the same axis spin in opposite directions. For such a configuration, a fixed-pitch quadcopter has an equilibrium when one motor fails.

Suppose propeller 1 of a conventional quadcopter fails to provide any thrust or torque. The dynamical model (1) and input equation (4) also apply to the conventional quadcopter. The only difference is that the pitch angles  $\alpha_i$  in (4) are identical and constant and hence could be merged with the coefficients  $k_i$  in (4) to form a new coefficient  $k_{ci}$ , where the subscript c denotes ‘‘conventional’’. Note that motor 2 and motor 4 spin in opposite directions such that there exists an equilibrium state when motor

1 fails. As a result, (4) becomes

$$\begin{aligned}
 u_{c1} &= k_{c1}(\omega_{c2}^2 + \omega_{c3}^2 + \omega_{c4}^2), \\
 u_{c2} &= k_{c1}\omega_{c3}^2, \\
 u_{c3} &= k_{c1}(\omega_{c4}^2 - \omega_{c2}^2), \\
 u_{c4} &= k_{c2}(\omega_{c3}^2 - \omega_{c2}^2 - \omega_{c4}^2) + \\
 &\quad k_{c3}(\omega_{c3} - \omega_{c2} - \omega_{c4}),
 \end{aligned} \tag{17}$$

with  $k_{c1}, k_{c2}, k_{c3}$  as constant parameters. As can be seen from (17),  $\omega_{ci}$  with  $i = 2, 3, 4$  are the independent control quantities. Denote  $\mathbf{z}_c = [\omega_{c2}, \omega_{c3}, \omega_{c4}]^T$ .

Next we need to identify the equilibrium point and linearise the model. Consider the equilibrium state

$$\mathbf{x}_c^* = [x_c^*, y_c^*, z_c^*, 0, 0, \psi_c^*, 0, 0, 0, 0, 0]^T.$$

It can be calculated that, in order to stay at the equilibrium state, the control quantities should be

$$\begin{aligned}
 \mathbf{z}_c^* &= [\omega_{c2}^*, \omega_{c3}^*, \omega_{c4}^*], \\
 &= \left[ \frac{mg}{2k_{c1}}, 0, \frac{mg}{2k_{c1}} \right].
 \end{aligned}$$

Let  $\bar{\mathbf{z}}_c = \mathbf{z}_c - \mathbf{z}_c^*$  and  $\bar{\mathbf{x}}_c = \mathbf{x}_c - \mathbf{x}_c^*$ . The linearised dynamical equation is

$$\dot{\bar{\mathbf{x}}}_c = \mathbf{A}_c \bar{\mathbf{x}}_c + \mathbf{B}_c \bar{\mathbf{z}}_c, \tag{18}$$

where

$$\begin{aligned}
 \mathbf{A}_c &= \left. \frac{\partial \mathbf{F}_c(\mathbf{x}_c, \mathbf{z}_c)}{\partial \mathbf{x}_c} \right|_{\mathbf{x}_c = \mathbf{x}_c^*, \mathbf{z}_c = \mathbf{z}_c^*} \\
 &= \begin{bmatrix} \mathbf{0}_{3 \times 3} & \mathbf{0}_{3 \times 3} & \mathbf{0}_{3 \times 3} & \mathbf{I}_{3 \times 3} \\ \mathbf{0}_{3 \times 3} & \mathbf{0}_{3 \times 3} & \mathbf{I}_{3 \times 3} & \mathbf{0}_{3 \times 3} \\ \mathbf{0}_{3 \times 3} & \mathbf{0}_{3 \times 3} & \mathbf{0}_{3 \times 3} & \mathbf{0}_{3 \times 3} \\ \mathbf{0}_{3 \times 3} & \mathbf{E}_{c3 \times 3} & \mathbf{0}_{3 \times 3} & \mathbf{0}_{3 \times 3} \end{bmatrix} \in \mathbb{R}^{12 \times 12}, \\
 \mathbf{E}_{c3 \times 3} &= \begin{bmatrix} g \sin \psi_c^* & g \cos \psi_c^* & 0 \\ -g \cos \psi_c^* & g \sin \psi_c^* & 0 \\ 0 & 0 & 0 \end{bmatrix},
 \end{aligned}$$

and

$$\begin{aligned}
 \mathbf{B}_c &= \left. \frac{\partial \mathbf{F}_c(\mathbf{x}_c, \mathbf{z}_c)}{\partial \mathbf{z}_c} \right|_{\mathbf{x}_c = \mathbf{x}_c^*, \mathbf{z}_c = \mathbf{z}_c^*} \\
 &= \begin{bmatrix} 0 & 0 & 0 \\ 0 & 0 & 0 \\ 0 & 0 & 0 \\ 0 & 0 & 0 \\ 0 & 0 & 0 \\ 0 & 0 & 0 \\ 0 & k_{c1}\omega_{c3}^* \frac{l}{I_x} & 0 \\ -k_{c1}\omega_{c2}^* \frac{l}{I_y} & 0 & k_{c1}\omega_{c4}^* \frac{l}{I_y} \\ r_2 & -r_3 & -r_4 \\ 0 & 0 & 0 \\ 0 & 0 & 0 \\ \frac{2k_{c1}}{m}\omega_{c2}^* & \frac{2k_{c1}}{m}\omega_{c3}^* & \frac{2k_{c1}}{m}\omega_{c4}^* \end{bmatrix} \in \mathbb{R}^{12 \times 3}, \\
 r_i &= -2k_{c2}\omega_{ci}^* + k_{c3} \frac{l}{I_z},
 \end{aligned}$$



with  $\mathbf{I}_{3 \times 3}$  as identity matrix.

Let  $k_{c1}l\omega_{c3}^*/I_x = c_1$ ,  $-k_{c1}l\omega_{c2}^*/I_y = c_2$ ,  $r_2 = r_4 = c_3$  and  $2k_{c1}\omega_{c2}^*/m = c_4$ . Then, the controllability matrix  $\mathbf{Q}_c$  is given in equation

$$\mathbf{Q}_c = [\mathbf{B}_c \ \mathbf{A}_c \mathbf{B}_c \ \mathbf{A}_c^2 \mathbf{B}_c \ \dots \ \mathbf{A}_c^{11} \mathbf{B}_c]$$

$$= \begin{bmatrix} 0 & 0 & 0 & 0 & 0 & 0 & 0 & 0 & 0 & -c_2 g & 0 & c_2 g \\ 0 & 0 & 0 & 0 & 0 & 0 & 0 & 0 & 0 & 0 & 0 & 0 \\ 0 & 0 & 0 & c_4 & 0 & c_4 & 0 & 0 & 0 & 0 & 0 & 0 \\ 0 & 0 & 0 & 0 & 0 & 0 & 0 & 0 & 0 & 0 & 0 & 0 \\ 0 & 0 & 0 & -c_2 & 0 & c_2 & 0 & 0 & 0 & 0 & 0 & 0 \\ 0 & 0 & 0 & c_3 & \frac{k_{c3}l}{I_z} & -c_3 & 0 & 0 & 0 & 0 & 0 & 0 \\ 0 & 0 & 0 & 0 & 0 & 0 & 0 & 0 & 0 & 0 & 0 & 0 \\ -c_2 & 0 & c_2 & 0 & 0 & 0 & 0 & 0 & 0 & 0 & 0 & 0 \\ c_3 & \frac{k_{c3}l}{I_z} & -c_3 & 0 & 0 & 0 & 0 & 0 & 0 & 0 & 0 & 0 \\ 0 & 0 & 0 & 0 & 0 & 0 & -c_2 g & 0 & c_2 g & 0 & 0 & 0 \\ 0 & 0 & 0 & 0 & 0 & 0 & 0 & 0 & 0 & 0 & 0 & 0 \\ c_4 & 0 & c_4 & 0 & 0 & 0 & 0 & 0 & 0 & 0 & 0 & 0 \end{bmatrix} \mathbf{0}_{12 \times 24}. \quad (19)$$

It can be counted that the rank of controllability matrix is  $\text{rank}(\mathbf{Q}_c) = 8$ . Since the full row rank of  $\mathbf{Q}_c$  is 12, the linearised system is not fully controllable and there are four uncontrollable modes.

Next, we conduct controllability decomposition to identify the uncontrollable states. Define a new state as  $\tilde{\mathbf{x}}_c = \mathbf{T}_c^{-1} \mathbf{x}_c$ , where  $\mathbf{T}_c$  is a transformation matrix. It follows from the linearised model in (18) that

$$\dot{\tilde{\mathbf{x}}}_c = \mathbf{T}_c^{-1} \mathbf{A}_c \mathbf{T}_c \tilde{\mathbf{x}}_c + \mathbf{T}_c^{-1} \mathbf{B}_c \tilde{\mathbf{z}}_c. \quad (20)$$

Following the controllability decomposition procedure<sup>21</sup>, take 10 linearly independent columns of (19) and add 4 custom columns to make  $\mathbf{T}_c$  nonsingular, as in

$$\mathbf{T}_c = \begin{bmatrix} 0 & 0 & 0 & 0 & 0 & 0 & 0 & -c_2 g & 0 & 0 & 0 & 0 \\ 0 & 0 & 0 & 0 & 0 & 0 & 0 & 0 & 1 & 0 & 0 & 0 \\ 0 & 0 & 0 & c_4 & 0 & c_4 & 0 & 0 & 0 & 0 & 0 & 0 \\ 0 & 0 & 0 & 0 & 0 & 0 & 0 & 0 & 0 & 1 & 0 & 0 \\ 0 & 0 & 0 & -c_2 & 0 & c_2 & 0 & 0 & 0 & 0 & 0 & 0 \\ 0 & 0 & 0 & c_3 & \frac{k_{c3}l}{I_z} & -c_3 & 0 & 0 & 0 & 0 & 0 & 0 \\ 0 & 0 & 0 & 0 & 0 & 0 & 0 & 0 & 0 & 0 & 1 & 0 \\ -c_2 & 0 & c_2 & 0 & 0 & 0 & 0 & 0 & 0 & 0 & 0 & 0 \\ c_3 & \frac{k_{c3}l}{I_z} & -c_3 & 0 & 0 & 0 & 0 & 0 & 0 & 0 & 0 & 0 \\ 0 & 0 & 0 & 0 & 0 & 0 & -c_2 g & 0 & 0 & 0 & 0 & 0 \\ 0 & 0 & 0 & 0 & 0 & 0 & 0 & 0 & 0 & 0 & 0 & 1 \\ c_4 & 0 & c_4 & 0 & 0 & 0 & 0 & 0 & 0 & 0 & 0 & 0 \end{bmatrix}. \quad (21)$$

Then, the new state could be partitioned into controllable component  $\tilde{\mathbf{x}}_c$  and uncontrollable component  $\tilde{\mathbf{x}}_{uc}$ , and (20) becomes

$$\begin{bmatrix} \tilde{\mathbf{x}}_c \\ \tilde{\mathbf{x}}_{uc} \end{bmatrix}' = \begin{bmatrix} \mathbf{A}_c & \mathbf{A}_{12} \\ \mathbf{0} & \mathbf{A}_{uc} \end{bmatrix} \begin{bmatrix} \tilde{\mathbf{x}}_c \\ \tilde{\mathbf{x}}_{uc} \end{bmatrix} + \begin{bmatrix} \mathbf{B}_c \\ \mathbf{0} \end{bmatrix} \tilde{\mathbf{z}}_c. \quad (22)$$

Substituting (21) into  $\tilde{\mathbf{x}}_c = \mathbf{T}_c^{-1} \tilde{\mathbf{x}}_c$  yields

$$\tilde{\mathbf{x}}_c = \begin{bmatrix} x_{12}m - x_8 \\ \frac{2c_4}{2c_2} - \frac{2c_2}{2c_4} \\ \frac{x_9}{x_8} + \frac{c_3 x_8}{c_2 c_5} \\ \frac{c_5}{x_8} + \frac{c_2 c_5}{x_{12}} \\ \frac{2c_2}{x_3} + \frac{2c_4}{x_5} \\ \frac{2c_4}{x_6} - \frac{2c_2}{x_5} \\ \frac{x_6}{x_5} + \frac{c_3 x_5}{c_2 c_5} \\ \frac{c_5}{x_5} + \frac{c_2 c_5}{x_3} \\ \frac{2c_2}{2c_2} + \frac{2c_4}{2c_4} \\ -\frac{x_{10}}{c_2 g} \\ -\frac{x_1}{c_2 g} \\ -c_2 g \\ x_2 \\ x_4 \\ x_7 \\ x_{11} \end{bmatrix}.$$

According to (22), the last four elements of  $\tilde{\mathbf{x}}_c$  correspond to uncontrollable modes. Hence  $x_2, x_4, x_7,$  and  $x_{11}$  are uncontrollable. Here,  $x_4$  and  $x_7$  represent  $\phi$  and  $p$ , respectively; and  $x_2$  and  $x_{11}$  represent  $y$  and  $v$ , respectively.

## 4 | CONTROLLER DESIGN AND SIMULATION VALIDATION

### 4.1 | Controller Design

Unlike conventional quadcopters, a VPP quadcopter remains controllable in the presence of one propeller failure. Therefore, simple LQR controllers can be designed based on the linearised model derived in preceding sections. This is an advantage of VPP quadcopters compared to the conventional ones.

### 4.2 | Simulation Examples

We next present three simulation examples to verify the effectiveness of the proposed results. In the simulation, suppose propeller 1 fails to work and hence it gives zero thrust force and zero torque. In the simulation, we model the actuator and speed control of a VPP as a first-order transfer function to approximate their dynamics. The cut-off frequency is chosen as 10 Hz.

#### 4.2.1 | Scenario 1: No Noise nor Disturbance

In this scenario, we assume that all the states can be measured perfectly and there are no external disturbances. The reference trajectory is a continuous circle combined with increasing altitude and varying orientation.

Simulation results are shown in Figs. 2 and 3. As can be seen, the quadcopter remains fully controllable though one propeller fails. Here, the reference tracking is achieved by tracking a moving target point with desired position and altitude.

#### 4.2.2 | Scenario 2: Measurements with Noise

In scenario 2, the quadcopter needs to track the target points varying from  $[0, 0, 0]$ ,  $[0, 0, 5]$ ,  $[5, 0, 5]$ , and finally to  $[5, 5, 5]$  at time  $t = 0, 2, 5, 10$ , respectively. The desired yaw angle changes from zero to 0.1 rad at  $t = 1$ . During the whole process, noise with the signal-to-noise ratio as 15 dB is added to all the feedback states.

Figs. 4 and 5 show the tracking performance of the VPP quadcopter. The quadcopter can quickly track the reference in the presence of noise.

#### 4.2.3 | Scenario 3: Noise and External Disturbance

In scenario 3, we assume that all the state measurements are corrupted by 15 dB signal-to-noise-ratio noise. More importantly, wind disturbance is considered. In particular, the wind disturbance is 4 m/s along x-axis and 4 m/s along y-axis when  $t \geq 1$ . The desired states are all set to 0. Fig. 6 presents the reaction of a VPP quadcopter facing an external disturbance and measurement

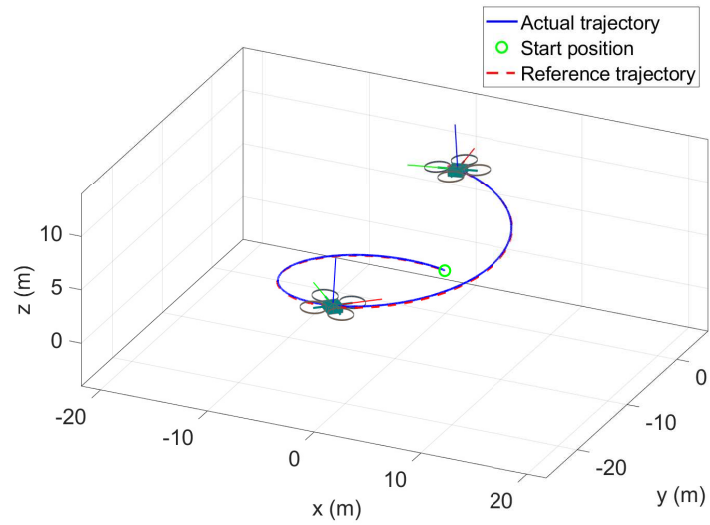


FIGURE 2 3D trajectory in scenario 1.

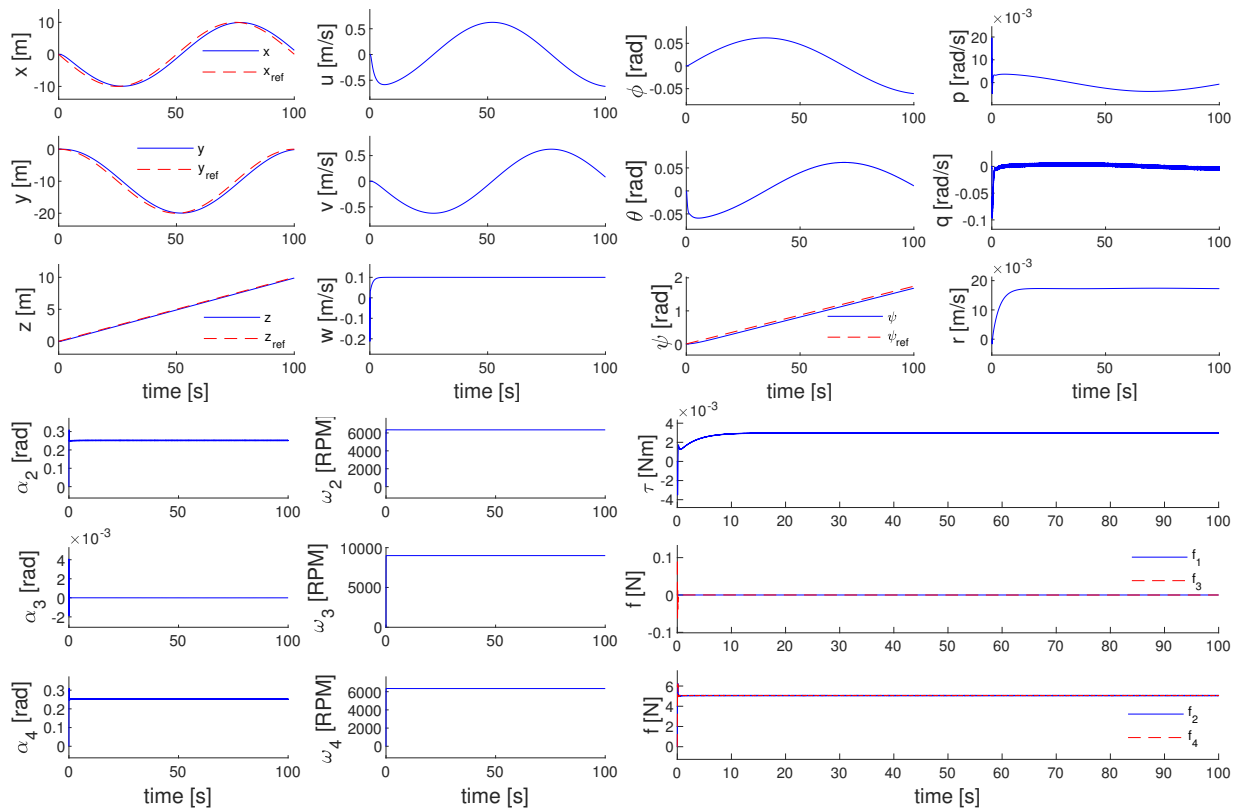


FIGURE 3 Simulation results for scenario 1.

noise. As can be seen in Fig. 7, the pitch and roll angles of the quadcopter converge to constant nonzero values to counter the wind disturbance.

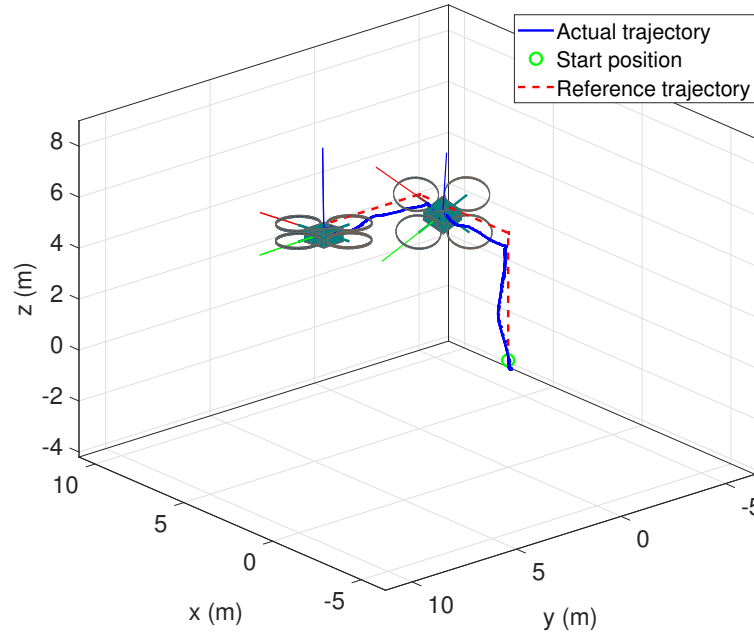


FIGURE 4 3D trajectory in scenario 2.

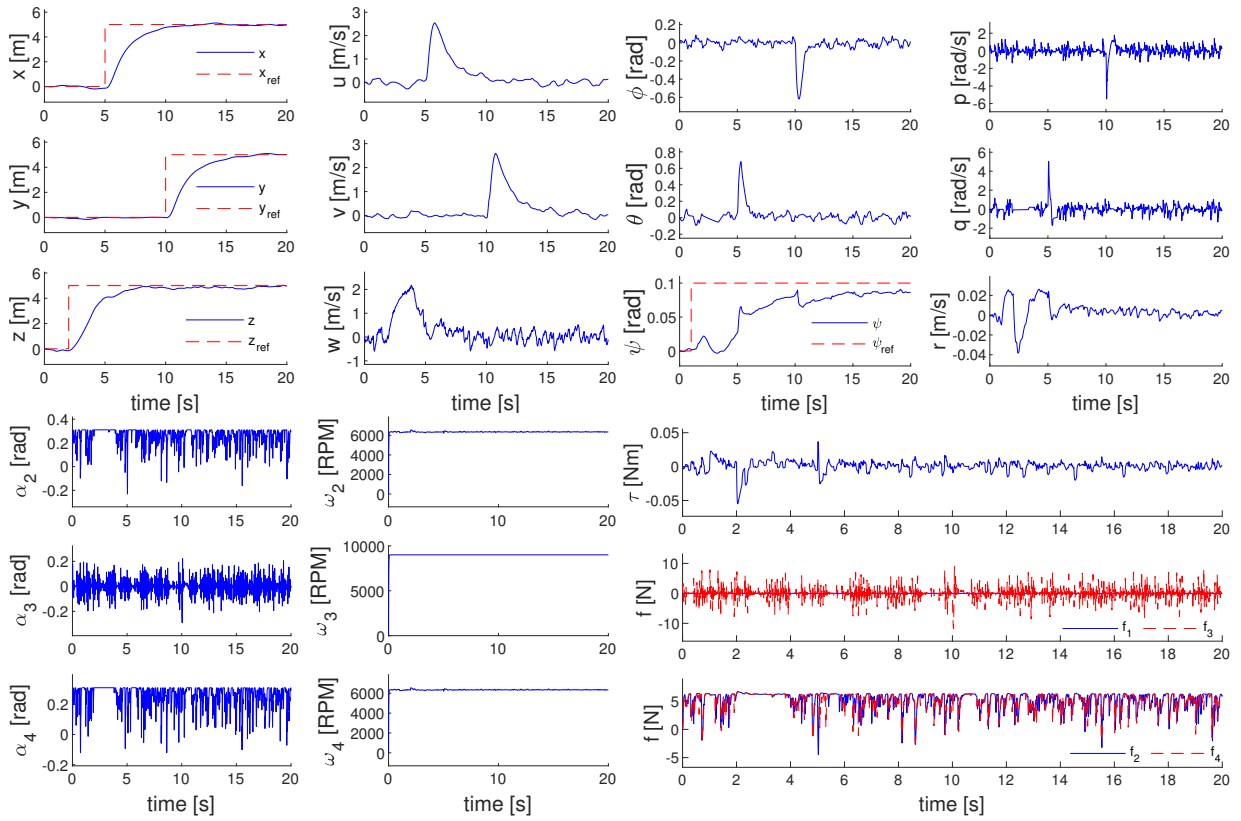


FIGURE 5 Simulation results for scenario 2.

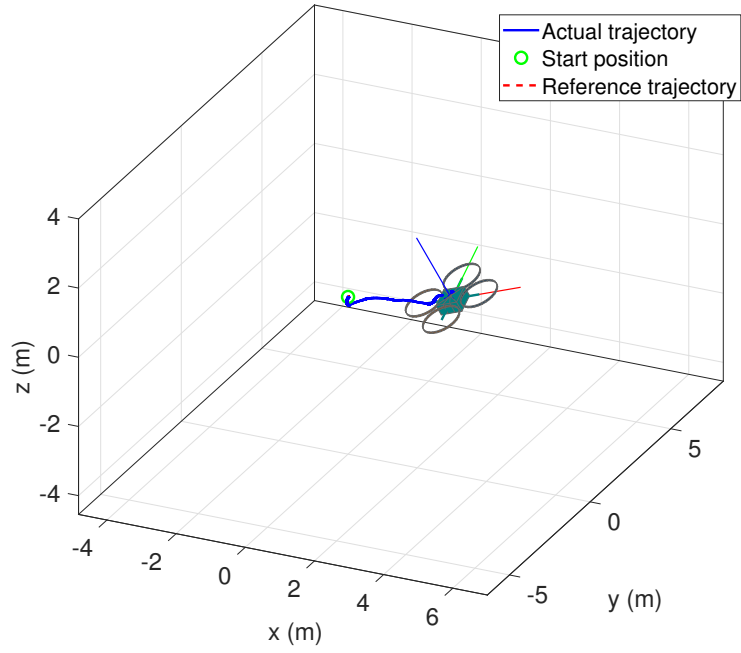


FIGURE 6 3D trajectory in scenario 3.

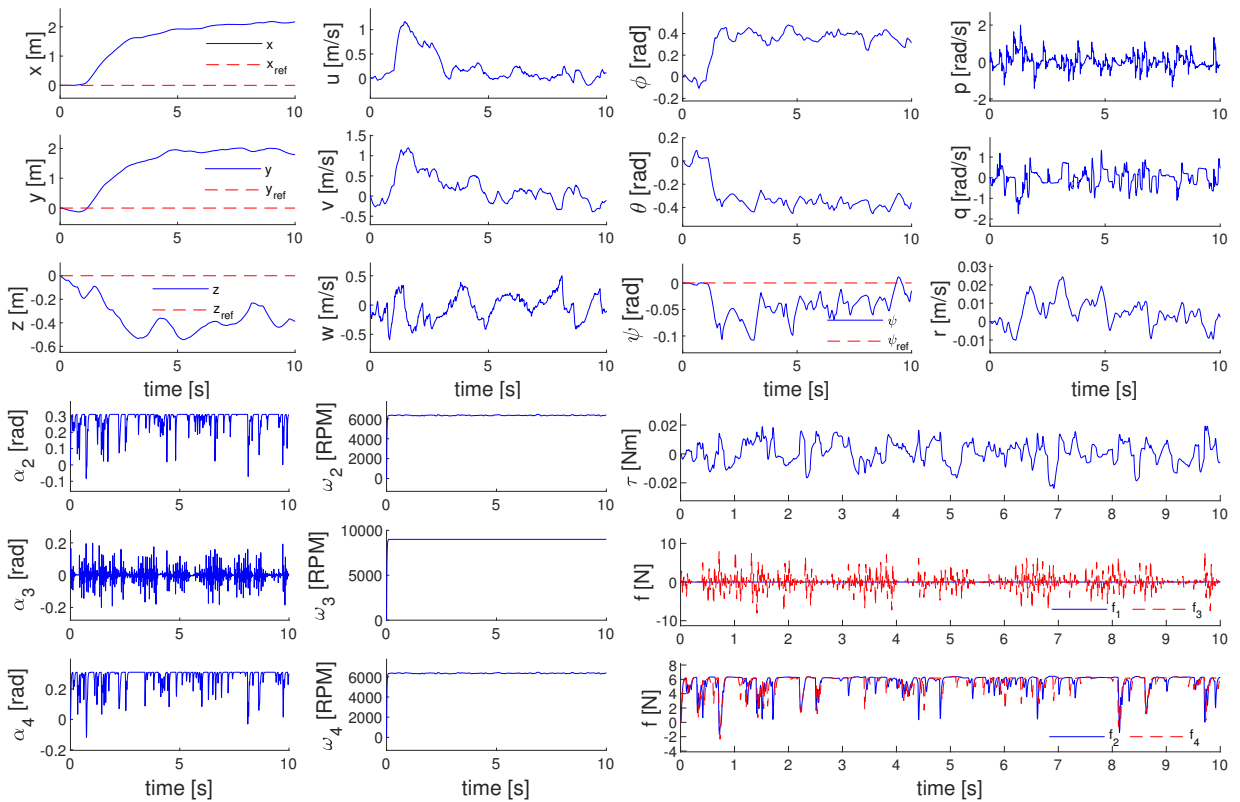


FIGURE 7 Simulation results for scenario 3.

## 5 | CONCLUSIONS

This paper studied the control of a VPP quadcopter in the presence of a propeller failure. It has been shown that the VPP quadcopter remains fully controllable and a simple LQR controller has been designed. Although the controllability analysis and controller design are both based on the linearised model, numerical simulation incorporating external disturbances and measurement noise has verified that the theoretical findings are still valid for the nonlinear dynamical model. It is suggested that VPP quadcopters provide a promising platform for various aerial tasks. The proposed controller could be extended to stabilise the quadcopter when the fault occurs during the normal flight in the future. In addition, we will study other fault-tolerant problems such as failure detection, isolation, and switching control of VPP quadcopters.

## References

1. Van M. An enhanced robust fault tolerant control based on an adaptive fuzzy pid-nonsingular fast terminal sliding mode control for uncertain nonlinear systems. *IEEE/ASME Transactions on Mechatronics* 2018; 23(3): 1362–1371.
2. Liu Z, Yuan C, Zhang Y, Luo J. A learning-based fault tolerant tracking control of an unmanned quadrotor helicopter. *Journal of Intelligent & Robotic Systems* 2016; 84(1-4): 145–162.
3. Sharifi F, Mirzaei M, Gordon BW, Zhang Y. Fault tolerant control of a quadrotor UAV using sliding mode control. In: *2010 Conference on Control and Fault-Tolerant Systems*; 2010: 239–244.
4. Zhang Y, Jiang J. Bibliographical review on reconfigurable fault-tolerant control systems. *Annual reviews in control* 2008; 32(2): 229–252.
5. Chen F, Jiang R, Zhang K, Jiang B, Tao G. Robust backstepping sliding-mode control and observer-based fault estimation for a quadrotor UAV. *IEEE Transactions on Industrial Electronics* 2016; 63(8): 5044–5056.
6. Zhong Y, Liu Z, Zhang Y, Zhang W, Zuo J. Active fault-tolerant tracking control of a quadrotor with model uncertainties and actuator faults. *Frontiers of Information Technology & Electronic Engineering* 2019; 20(1): 95–106.
7. Chamseddine A, Theilliol D, Zhang Y, Join C, Rabbath CA. Active fault-tolerant control system design with trajectory re-planning against actuator faults and saturation: Application to a quadrotor unmanned aerial vehicle. *International Journal of Adaptive Control and Signal Processing* 2015; 29(1): 1–23.
8. Cutler M, Ure NK, Michini B, How J. Comparison of fixed and variable pitch actuators for agile quadrotors. In: *Proceedings of AIAA Guidance, Navigation, and Control Conference*; 2011: 6406–6423.
9. Cutler M, How J. Actuator constrained trajectory generation and control for variable-pitch quadrotors. In: *Proceedings of AIAA Guidance, Navigation, and Control Conference*; 2012: 4777–4792.
10. Cutler M, How JP. Analysis and control of a variable-pitch quadrotor for agile flight. *Journal of Dynamic Systems, Measurement, and Control* 2015; 137(10): 101002–101016.
11. Gupta N, Kothari M, others . Flight dynamics and nonlinear control design for variable-pitch quadrotors. In: *Proceedings of 2016 American Control Conference (ACC)IEEE*. ; 2016: 3150–3155.
12. Sheng S, Sun C. Control and optimization of a variable-pitch quadrotor with minimum power consumption. *Energies* 2016; 9(4): 232–250.
13. Mueller MW, D’Andrea R. Stability and control of a quadcopter despite the complete loss of one, two, or three propellers. In: *Proceedings of 2014 IEEE International Conference on Robotics and Automation*; 2014: 45–52.
14. Qi X, Qi J, Theilliol D, Song D, Zhang Y, Han J. Self-healing control design under actuator fault occurrence on single-rotor unmanned helicopters. *Journal of Intelligent & Robotic Systems* 2016; 84(1-4): 21–35.
15. Freddi A, Lanzon A, Longhi S. A feedback linearization approach to fault tolerance in quadrotor vehicles. *IFAC proceedings volumes* 2011; 44(1): 5413–5418.

16. Mueller MW, D'Andrea R. Relaxed hover solutions for multicopters: Application to algorithmic redundancy and novel vehicles. *The International Journal of Robotics Research* 2016; 35(8): 873–889.
17. Merheb AR, Noura H, Bateman F. Emergency control of AR drone quadrotor UAV suffering a total loss of one rotor. *IEEE/ASME Transactions on Mechatronics* 2017; 22(2): 961–971.
18. Bristeau P, Martin P, Salaün E, Petit N. The role of propeller aerodynamics in the model of a quadrotor UAV. In: *Proceedings of 2009 European Control Conference*; 2009: 683–688.
19. Powers C, Mellinger D, Kushleyev A, Kothmann B, Kumar V. Influence of aerodynamics and proximity effects in quadrotor flight. In: Desai JP, Dudek G, Khatib O, Kumar V., eds. *Springer Tracts in Advanced Robotics*. 88. Springer, Heidelberg. 2013 (pp. 289–302).
20. Ent CY. Stingray 500. 2016. Accessed: 2019-09-1.
21. Boley D. Computing the Kalman decomposition: An optimal method. *IEEE Transactions on Automatic Control* 1984; 29(1): 51–53.

